

SEMI-ANALYTICAL SOLUTION OF THE ϕ^4 THEORY ON AN F_4 LATTICE

Markus Klomfass ¹

Department of Physics, Columbia University, New York, NY 10027, USA

ABSTRACT

Investigating the cutoff dependence of the Higgs mass triviality bound, the ϕ^4 theory is formulated on an F_4 lattice which preserves Lorentz invariance to a higher degree than the commonly used hypercubic lattice. I solve this model non-perturbatively by evaluating the high temperature expansion through 13th order following the approach of Lüscher and Weisz. The results are continued across the transition line into the broken phase by integrating the perturbative RG equations. In the broken phase, the renormalized coupling never exceeds $2/3$ of the tree level unitarity bound when $\Lambda/m_R \geq 2$. The results confirm recent Monte Carlo data and I obtain as an upper bound for the Higgs mass $m_R/f_\pi \leq 2.46 \pm 0.02_{\text{HTE}} \pm 0.08_{\text{PT}}$ at $\Lambda/m_R = 2$.

¹e-mail: klomfass@cuphyg.phys.columbia.edu

1 Introduction

The relevance of the cutoff within the ϕ^4 theory arises because of triviality, i.e. the vanishing of the self-coupling in the continuum limit. If the model were not trivial, all one would be interested in would be the continuum limit, which of course is cutoff independent, and thus this investigation into the cutoff dependence of the Higgs mass bound would be irrelevant. Because of triviality, the cutoff has to be kept finite in order to retain a meaningful model at non-zero coupling. In this way, the Standard Model has to be viewed as an effective low energy theory with a built in cutoff, embedded in some yet unknown full theory. For self consistency, this cutoff should be at least a few times the Higgs mass, beyond the particle content of the effective theory. The closer the Higgs lies to the cutoff scale, the more important the effects of the embedding theory (i.e. the cutoff effects) will be. Thus a search for a maximal Higgs mass demands a careful investigation of the cutoff dependence on the triviality bound.

To lowest order in the cutoff, the scalar sector is described accurately by the usual ϕ^4 Lagrangian. The effect of the underlying full theory is to introduce corrections in the form of (yet unknown) higher dimensional operators. There are two dimension six operators parameterizing the leading order (Λ^{-2}) cutoff effects. The ordinary hypercubic lattice — which is commonly used in Monte Carlo investigations of the Higgs bound — breaks Lorentz invariance already at order Λ^{-2} , so the cutoff dependence on the lattice could look very different than in the real world. The hypercubic lattice regularization could severely contaminate the physics. The F_4 lattice, in contrast, accurately reproduces all physical $\mathcal{O}(\Lambda^{-2})$ corrections and Lorentz breaking effects first occur at order Λ^{-4} . Scalar fields can be implemented trivially on the F_4 lattice. This idea was first suggested by Neuberger [1].

Despite triviality, the cutoff may turn out to be so low that the physical self-coupling could indeed be strong (with respect to a tree level unitarity bound). This calls for non-perturbative methods to investigate the triviality bound, even though previous work on a hypercubic lattice seems not to leave much room for a strongly coupled scalar sector. Besides Monte Carlo methods, where systematic errors arise because of the finite system size, the strong coupling (or high-temperature) expansion has been worked out. Here results are obtained directly in the infinite volume limit, without any statistical errors. The method, however, only works in the symmetric phase and relies on the perturbative renormalization group to be continued into the Goldstone phase. It is also quite cumbersome to apply the high-temperature expansion to lattice actions that include additional higher dimensional operators which modify the naive nearest neighbor interaction.

Monte Carlo simulations have been previously performed on an F_4 lattice, but a strong coupling expansion of the model on this particular lattice has been lacking so far. I will essentially follow the approach of Lüscher and Weisz, presented in a series of papers [2,3,4,5] and extend the application to the F_4 lattice. For completeness, I will repeat some of their techniques and emphasize the adaptations necessary for the F_4 lattice.

I work within the Dashen-Neuberger approximation [6], i.e. Gauge and Yukawa couplings are neglected. They are weak and may be included later via perturbation theory. This approximation holds (i.e. captures the relevant physics) if the top quark is well below 0.5 TeV (which seems to be favored by experiment). In this limit the Higgs action turns into

the action for an O(4)-symmetric ϕ^4 model

$$S_H = \int d^4x \left\{ \frac{1}{2} \partial_\mu \phi \cdot \partial_\mu \phi + \frac{\lambda}{8} (\phi^2 - v^2)^2 \right\}. \quad (1)$$

The two physical scales in the broken phase are set by the Higgs mass and the pion decay constant $f_\pi = 246$ GeV. Based on f_π , a physical self-coupling g_R is defined as

$$g_R = 3 \left(\frac{m_R}{f_\pi} \right)^2. \quad (2)$$

Triviality of ϕ^4 in four dimensions is not rigorously proven but rests on perturbative renormalization group (RG) results and Monte Carlo data [7,8,9,10,11]. Perturbative renormalization group leads to the relation

$$m_R/\Lambda = C_1 (\beta_1 g_R)^{-\beta_2/\beta_1^2} \exp \left(-\frac{1}{\beta_1 g_R} \right) \{1 + \mathcal{O}(g_R)\} \quad \text{as } g_R \rightarrow 0, \quad (3)$$

with C_1 being a λ -dependent integration constant that will be evaluated in the high-temperature expansion. Removal of the cutoff Λ will lead to a trivial theory. Lowering the cutoff, however, g_R is increasing accordingly. But so are cutoff effects and by putting a limit on the acceptable cutoff dependence in physical observables (for instance pion–pion scattering at 90 degrees) one gets an upper bound on g_R and hence on m_R/f_π defined in a *lattice independent* way, valid beyond the realms of lattice gauge theory.

The smaller the coefficient C_1 in (3) (which depends on the higher dimensional operators in an improved action) the less the impact a change in the cutoff will have on m_R/f_π . This in turn allows a higher mass bound. I refer to [12,13,14] for a detailed analysis.

This paper is organized as follows. In the next section I will briefly review some perturbative results for the ϕ^4 model on an F_4 lattice. I will give scaling laws in the symmetric and in the broken phase. (Expressions up to three loops for the RG functions are listed in the appendix.) These results were worked out by Lüscher and Weisz [2,3,4,5] and by Bhanot et al. [12,13]. In the following section, I will give a detailed account of the high-temperature series in form of a linked cluster expansion. The method follows work by Lüscher and Weisz (henceforth referred to as LW) [2], but is adapted to the F_4 lattice. The analysis of the expansion up to 13th order is presented in the last section (preliminary results were given in [15,16]). Results in the broken phase are obtained by propagating the high-temperature expansion results using the perturbative RG equations given in section 2. I will show that the region where the cluster expansion converges and the perturbative region do overlap on the F_4 lattice. An estimate for the Higgs triviality bound is given and compared with Monte Carlo data. Ultimately, this comparison serves as an indicator of the size of systematic errors. Furthermore, the F_4 result shows that Lorentz invariance breaking effects are less than 10%, indicating the robustness of the triviality bound.

2 Definitions, scaling laws and matching

Many of the perturbative results required for the high-temperature expansion analysis listed throughout this section are taken from [5] and [12] and are reproduced here for completeness only.

The naive euclidean lattice action for the ϕ^4 theory is

$$S = -2\kappa \sum_{\langle xx' \rangle} \phi(x)\phi(x') + \sum_x u(\phi(x)), \quad (4)$$

with a local $O(N)$ invariant potential

$$u(\phi) = \phi^2 + \lambda(\phi^2 - 1)^2. \quad (5)$$

The summation in (4) is over all nearest neighbor pairs $\langle xx' \rangle$ and ϕ is a real N -component field $\phi^a(x)$, $a = 1, \dots, N$, located on an F_d lattice. The parameter range is restricted to $\kappa \geq 0$ and $\lambda \geq 0$. The model is known to exist in two phases, separated by a second order critical line $\kappa_c(\lambda)$.

The F_d lattice in $d \geq 2$ dimensions is defined as the set of points $\{x|x = \sum_\mu x_\mu e_{(\mu)}, x_\mu \in \mathbb{Z}, \sum_\mu x_\mu = \text{even}\}$. Here $e_{(\mu)}$ is the euclidean unit vector in the μ -direction. F_d can be viewed as a hypercubic lattice \mathbb{Z}^d with its odd sites removed and for $d = 3$ it corresponds to an *fcc* lattice. The euclidian distance between nearest neighbors is $\sqrt{2}$ and there are $2d(d-1)$ nearest neighbors per site. The discrete rotation symmetry group is particularly large in four dimensions and in this case the Lorentz invariance breaking term in the kinetic energy part of the free propagator vanishes. Invariance breaking terms first occur at order Λ^{-4} .

The generating functional W for the connected correlation functions of ϕ and \mathcal{O} in the presence of the external sources $J(x)$ and $K(x)$ is

$$\exp(W[J, K]) = \frac{1}{Z[0, 0]} \int \prod_{x, \alpha} d\phi^\alpha(x) \exp \left\{ -S[\phi] + \sum_{x, \beta} J^\beta(x)\phi^\beta(x) + \sum_x K(x)\mathcal{O}(x) \right\}, \quad (6)$$

where \mathcal{O} is a composite operator defined as $\mathcal{O}(x) = 2\sum_{\langle xx' \rangle} \phi(x)\phi(x')$. The connected correlation functions are then obtained by taking the derivatives of $W[J, K]$ with respect to the sources

$$W^{(n, l)}(x_1, \dots, x_n; y_1, \dots, y_l)_{\alpha_1 \dots \alpha_n} = \frac{\delta^{n+l}}{\delta J_{\alpha_1}(x_1) \dots \delta J_{\alpha_n}(x_n) \delta K(y_1) \dots \delta K(y_l)} W[J, K] \Big|_{J=K=0}. \quad (7)$$

The vertex functions $\Gamma^{(n, l)}$ are generated by the one particle irreducible functional $\Gamma[M, K]$ defined as the Legendre transform $\Gamma = W - \sum_x J(x)M(x)$. Then

$$\Gamma^{(n, l)}(p_1, \dots, p_n; q_1, \dots, q_l)_{\alpha_1 \dots \alpha_n} = \frac{\delta^{n+l}}{\delta \tilde{M}(p_1)_{\alpha_1} \dots \delta \tilde{M}(p_n)_{\alpha_n} \delta \tilde{K}(q_1) \dots \delta \tilde{K}(q_l)} \Gamma[M, K] \Big|_{M=K=0}, \quad (8)$$

and M is the local magnetization, $M = \partial W / \partial J$. Because of $O(N)$ invariance, the coefficients $\Gamma^{(n, l)}$ vanish for odd n .

The renormalization conditions imposed on the vertex functions in the symmetric phase at zero external momentum define the wavefunction renormalization constant Z_R and the renormalized mass m_R ,

$$\Gamma^{(2, 0)}(p, -p)_{\alpha\beta} = \delta_{\alpha\beta} \frac{1}{Z_R} \{p^2 + m_R^2\} + \mathcal{O}(p^4), \quad (p \rightarrow 0). \quad (9)$$

The renormalized coupling is fixed via

$$\Gamma^{(4,0)}(0,0,0,0)_{\alpha\beta\gamma\delta} = \frac{1}{3}C_4(\alpha, \beta, \gamma, \delta)\frac{g_R}{Z_R^2}, \quad (10)$$

with C_4 being the totally symmetric $O(N)$ invariant tensor $C_4(\alpha, \beta, \gamma, \delta) = \delta_{\alpha\beta}\delta_{\gamma\delta} + \delta_{\alpha\gamma}\delta_{\beta\delta} + \delta_{\alpha\delta}\delta_{\beta\gamma}$. The field renormalization constant $Z_R^{\mathcal{O}}$ associated with the composite operator \mathcal{O} is given by

$$\Gamma^{(2,1)}(0,0;0)_{\alpha\beta} = \delta_{\alpha\beta}\frac{1}{Z_R Z_R^{\mathcal{O}}}. \quad (11)$$

The renormalized vertex functions are defined by

$$\begin{aligned} \Gamma_R^{(n,l)} &= 0 \quad \text{for odd } n \text{ and for } n=0, l \leq 1, \\ \Gamma_R^{(n,l)} &= Z_R^{n/2} Z_R^{\mathcal{O}l} \left\{ \Gamma^{(n,l)} - \delta_{n0} \delta_{l2} \Gamma^{(0,2)}(0,0) \right\} \quad \text{otherwise,} \end{aligned} \quad (12)$$

and satisfy the following normalization conditions

$$\Gamma_R^{(2,0)}(p, -p)_{\alpha\beta} = \delta_{\alpha\beta} \{p^2 + m_R^2\} + \mathcal{O}(p^4), \quad (p \rightarrow 0), \quad (13)$$

$$\Gamma_R^{(4,0)}(0,0,0,0)_{\alpha\beta\gamma\delta} = \frac{1}{3}C_4(\alpha, \beta, \gamma, \delta)g_R, \quad (14)$$

$$\Gamma_R^{(0,2)}(0,0) = 0, \quad (15)$$

$$\Gamma_R^{(2,1)}(0,0;0)_{\alpha\beta} = \delta_{\alpha\beta}. \quad (16)$$

From the lattice action, the vertex functions will be expressed in terms of κ and λ . Taking the derivative of the renormalized vertex functions with respect to κ at a fixed value of λ , one derives the *Callan-Symanzik* equation

$$\begin{aligned} &\left\{ m_R \frac{\partial}{\partial m_R} + \beta \frac{\partial}{\partial g_R} - n\gamma - l\delta \right\} \Gamma_R^{(n,l)} \\ &= \epsilon m_R^2 \left\{ \Gamma_R^{(n,l+1)} \Big|_{q_{l+1}=0} - \delta_{n0} \delta_{l2} \Gamma_R^{(0,3)}(0,0,0) \right\}. \end{aligned} \quad (17)$$

The coefficients are defined by

$$\beta(m_R, g_R) = m_R \frac{\partial g_R}{\partial \kappa} \Big/ \frac{\partial m_R}{\partial \kappa}, \quad (18)$$

$$\gamma(m_R, g_R) = \frac{1}{2} m_R \frac{\partial \ln Z_R}{\partial \kappa} \Big/ \frac{\partial m_R}{\partial \kappa}, \quad (19)$$

$$\delta(m_R, g_R) = m_R \frac{\partial \ln Z_R^{\mathcal{O}}}{\partial \kappa} \Big/ \frac{\partial m_R}{\partial \kappa}, \quad (20)$$

$$\epsilon(m_R, g_R) = \left(m_R Z_R^{\mathcal{O}} \frac{\partial m_R}{\partial \kappa} \right)^{-1} = 2(\gamma - 1). \quad (21)$$

Equivalently, one may write the above equations in the following way

$$m_R \frac{\partial g_R}{\partial m_R} = \beta, \quad (22)$$

$$m_R \frac{\partial \ln Z_R}{\partial m_R} = 2\gamma, \quad (23)$$

$$m_R \frac{\partial \ln Z_R^{\mathcal{O}}}{\partial m_R} = \delta, \quad (24)$$

$$m_R \frac{\partial \kappa}{\partial m_R} = m_R^2 \epsilon Z_R^{\mathcal{O}}, \quad (25)$$

where all derivatives are taken at fixed λ and m_R is the independent variable. At the transition, as $m_R \rightarrow 0$, the RG functions β, γ, δ and ϵ have finite limits. The universal coefficients $\beta_\nu, \gamma_\nu, \delta_\nu$ and ϵ_ν have been previously calculated up to three loops. They are given in the appendix together with the non-universal scaling violating terms up to one loop.

Equation (22) implies that, for a positive β -function, as $m_R \rightarrow 0$ the coupling also tends to zero as given in eq. (3). Similarly, scaling laws for $Z_R, Z_R^{\mathcal{O}}$ and κ are derived from eqs. (23)–(25). Specifically, one has

$$Z_R = C_2 \{1 + \mathcal{O}(g_R)\}, \quad (26)$$

$$Z_R^{\mathcal{O}} = C_3 (g_R)^{\delta_1/\beta_1} \{1 + \mathcal{O}(g_R)\}, \quad (27)$$

$$\kappa_c - \kappa = C_3 m_R^2 (g_R)^{\delta_1/\beta_1} \{1 + \mathcal{O}(g_R)\}. \quad (28)$$

Switching from m_R to a new independent variable $\tau = 1 - \kappa/\kappa_c$, the equations are transformed to

$$m_R \stackrel{\tau \rightarrow 0}{\sim} C_4 \tau^{1/2} |\ln \tau|^{\delta_1/2\beta_1}, \quad (29)$$

$$g_R \stackrel{\tau \rightarrow 0}{\sim} \frac{2}{\beta_1} |\ln \tau|^{-1}, \quad (30)$$

$$Z_R \stackrel{\tau \rightarrow 0}{\sim} C_2, \quad (31)$$

$$Z_R^{\mathcal{O}} \stackrel{\tau \rightarrow 0}{\sim} C_5 |\ln \tau|^{-\delta_1/\beta_1}. \quad (32)$$

At this point, note that the susceptibility (as defined in (46) below) is related to the renormalized quantities via $\chi_2 = Z_R m_R^{-2}$, resulting in the following scaling behavior

$$\chi_2 \stackrel{\tau \rightarrow 0}{\sim} C_6 \tau^{-1} |\ln \tau|^{-\delta_1/\beta_1}. \quad (33)$$

At small λ however, the divergence of the susceptibility is dominated by the τ^{-1} term, unless one is very close to the critical line. This can be seen as follows. Keeping terms proportional to the initial value $g_0 = 6\lambda/(d-1)^2 \kappa^2$ when integrating the RG equations, one obtains

$$g_R \stackrel{\tau \rightarrow 0}{\sim} g_0 \left\{ 1 + \frac{\beta_1 g_0}{2} |\ln \tau| \right\}^{-1}, \quad (34)$$

and thus the improved scaling law for the susceptibility

$$\chi_2 \stackrel{\tau \rightarrow 0}{\sim} C_7 \tau^{-1} \left(1 - f(\lambda) |\ln \tau|\right)^{-\delta_1/\beta_1}. \quad (35)$$

Here I have defined

$$f(\lambda) = \frac{d^2}{4\pi^2} \frac{N+8}{N+2} \bar{\lambda} + \mathcal{O}(\bar{\lambda}^2), \quad (36)$$

where $\bar{\lambda} = (N+2)\lambda + \mathcal{O}(\lambda^2)$ (see (79) for a proper definition) and I used the fact that κ is close to $\kappa_c = 1/2d(d-1) + \mathcal{O}(\lambda)$. All the other scaling laws are modified accordingly. The improvement indicates that the logarithmic divergence is suppressed for small λ .

In the broken symmetry phase, the N -th component of ϕ is given a vacuum expectation value v while the first $N-1$ components remain massless. The generating functionals are defined in the limit of a vanishing external magnetic field h . The vertex functions $\Gamma^{(n,l)}$ are again given by (8). However, in the broken phase they are only $O(N-1)$ invariant. The perturbative expansion of the vertex functions in the broken phase is defined around $\phi_\alpha = \delta_{\alpha N} s_{\min}$, where s_{\min} is one of the two degenerate absolute minima of the lattice action.

The renormalization conditions in the broken phase are imposed (following [12]) as

$$\Gamma_R^{(2,0)}(p, -p)_{\alpha\beta} = \delta_{\alpha\beta} p^2 + \mathcal{O}(p^4), \quad (p \rightarrow 0), \quad (37)$$

$$\text{Re} \left\{ \Gamma^{(2,0)}(p, -p)_{NN} \Big|_{p=(im_R, 0, 0, 0)} \right\} = 0, \quad (38)$$

$$\text{Re} \left\{ \Gamma^{(1,1)}(p; -p)_N \Big|_{p=(im_R, 0, 0, 0)} \right\} = \frac{v}{Z_R Z_R^{\mathcal{O}}}. \quad (39)$$

The pion decay constant is just the vacuum expectation value of the renormalized σ -field $f_\pi = (Z_R)^{-\frac{1}{2}} v$. Now the renormalized self-coupling is defined as in eq. (2) and renormalized vertex functions are introduced via

$$\begin{aligned} \Gamma_R^{(n,l)} &= 0 \quad \text{for } n=0, l \leq 1, \\ \Gamma_R^{(n,l)} &= Z_R^{n/2} Z_R^{\mathcal{O}l} \left\{ \Gamma^{(n,l)} - \delta_{n0} \delta_{l2} \Gamma^{(0,2)}(p, -p) \Big|_{p=(im_R, 0, 0, 0)} \right\} \quad \text{otherwise.} \end{aligned} \quad (40)$$

The Callan-Symanzik equation in the broken phase reads

$$\begin{aligned} \left\{ m_R \frac{\partial}{\partial m_R} + \beta \frac{\partial}{\partial g_R} - n\gamma - l\delta \right\} \Gamma_R^{(n,l)} \\ = \vartheta m_R \Gamma_R^{(n+1,l)} \Big|_{p_{n+1}=0, \alpha_{n+1}=N} + \epsilon m_R^2 \Gamma_R^{(n,l+1)} \Big|_{q_{l+1}=0} \end{aligned} \quad (41)$$

The RG functions are defined as in eqs. (18)–(21). However, the relation between ϵ and γ is not valid in the broken phase, and — unfortunately — in the case of $N=4$ there exists no simple relation between ϵ and the other RG functions. The function ϑ is defined as

$$\vartheta(m_R, g_R) = Z_R^{-1/2} \frac{\partial v}{\partial \kappa} \Big/ \frac{\partial m_R}{\partial \kappa}, \quad (42)$$

and it is related to the other functions through

$$\vartheta = \left(1 + \gamma - \frac{1}{2g_R}\beta\right) \sqrt{\frac{3}{g_R}}. \quad (43)$$

The universal coefficients $\beta_\nu, \gamma_\nu, \delta_\nu$ and ϵ_ν plus the scaling violating terms are listed in the appendix.

The scaling laws for m_R , Z_R , and $Z_R^{\mathcal{O}}$ — given in (3), (26) and (27) — are exactly the same, except with integration constants C'_i instead of C_i . The only change is that in the scaling law (28) for κ appears an additional factor of $-1/2$

$$\kappa - \kappa_c = \frac{1}{2} C'_3 m_R^2 (g_R)^{\delta_1/\beta_1} \{1 + \mathcal{O}(g_R)\}. \quad (44)$$

As in the symmetric phase, the scaling law for m_R implies that the renormalized coupling tends to zero when approaching the critical line from above.

To connect the theory in the symmetric with the theory in the broken phase, one has to establish a relationship between the integration constants C_i and C'_i on both sides of the transition. This is accomplished by reconstructing the massive renormalized vertex functions in both phases from the critical renormalized vertex functions by mass perturbation theory. The answer can be obtained from a one-loop calculation. One finds

$$C'_1(\lambda) = C_1(\lambda) \exp\left\{\frac{2N + 17 - 3\sqrt{3}\pi}{2N + 16}\right\}, \quad (45)$$

and $C'_i = C_i$ for $i = 2, 3$.

Finally, the tree level unitarity bound in the symmetric phase from the S -wave phase shift for elastic scattering amounts to $g_R < 29$ for $N = 4$. An almost equal bound holds in the broken phase [5].

3 The linked cluster expansion

As a powerful non-perturbative semi-analytical tool, the high-temperature expansion serves as an alternative to Monte Carlo methods. It has been widely used and for details I refer to [2, 17]. The high-temperature expansion can be systematically organized in terms of graphs consisting of vertices and connecting lines. This method is referred to as *linked cluster expansion*. The number of lines in a graph corresponds to the power of the hopping parameter κ in the high-temperature expansion. I compute susceptibilities up to 13th order in κ with a total of about 400 000 contributing graphs. The number of contributing graphs depends on the lattice structure as not all graphs can be embedded on all lattices. The whole procedure is computerized as outlined in [2] and is easily adaptable for different potentials and lattice structures.

It is sufficient to define the following susceptibilities in terms of the connected correlation functions $W^{(2,0)}$ and $W^{(4,0)}$

$$\chi_2 = \frac{1}{N} \sum_{x,a} \langle \phi^a(x) \phi^a(0) \rangle^{\text{conn}}, \quad (46)$$

$$\mu_2 = \frac{1}{N} \sum_{x,a} x^2 \langle \phi^a(x) \phi^a(0) \rangle^{\text{conn}}, \quad (47)$$

$$\chi_4 = \frac{1}{N^2} \sum_{\substack{x,y,z \\ a,b}} \langle \phi^a(x) \phi^a(y) \phi^b(z) \phi^b(0) \rangle^{\text{conn}}, \quad (48)$$

where the spatial summation produces zero momentum operators. From the expansion of the susceptibilities an expansion for the quantities of interest, particularly the mass m_R , the coupling g_R , and the wavefunction renormalization constants Z_R and $Z_R^{\mathcal{O}}$ can be calculated in principal anywhere in the symmetric phase via

$$m_R = \left(2d \frac{\chi_2}{2\mu_2} \right)^{1/2}, \quad (49)$$

$$g_R = -(2d)^2 \frac{\chi_4}{2\mu_2^2}, \quad (50)$$

$$Z_R = 2d \frac{\chi_2^2}{\mu_2}, \quad (51)$$

$$Z_R^{\mathcal{O}} = \frac{\mu_2}{d} \left(\frac{\partial \chi_2}{\partial \kappa} \right)^{-1}. \quad (52)$$

These relations can easily be derived from the renormalization conditions imposed on the vertex functions in the symmetric phase. To extend the solution into the broken phase one has to resort to other means, e.g. perturbative RG techniques.

Care has to be taken in defining a proper Fourier transform on the underlying lattice structure. The particular form of the Brillouin zone on the F_4 lattice results in additional factors of 2 in the above relations as compared to the hypercubic case.

I will now introduce the necessary ingredients for the cluster expansion, starting with some basic definitions. A graph G is defined by a set $(\mathcal{V}, \mathcal{L}, \mathcal{E})$, where \mathcal{V} represents the *vertices*, \mathcal{L} the *internal lines* connecting the vertices and \mathcal{E} the number of *external lines* attached to each vertex. Let V be the total number of vertices, L the number of internal lines or *order* of the graph, E the total number of external lines. Let $N(v) = I(v) + E(v)$ be the total number of lines, internal plus external, attached to a vertex v . Two graphs G and G' are called *topologically equivalent*, if G' can be transformed into G by simply reordering its vertices and $[G]$ is the corresponding equivalence class of graphs. In the linked cluster expansion, the particular order of the vertices is irrelevant and therefore the expansion is in terms of equivalent classes rather than individual graphs. Care has to be taken to avoid overcounting.

The *distance* between two vertices $d(v_i, v_j)$ is the length of the shortest path between v_i and v_j . A *loop* is a closed path. Generally, a graph may contain vertices that are not connected by a path to some (or all) other vertices. A graph G is said to be *connected* if there is at least one path between any two vertices. A connected graph G is said to be *non-separable* if for all vertices v the graph G remains connected after removal of v and all lines emanating from it. A graph is called *simple* if any two vertices are connected by at most one line and there are no self-loops (i.e. no lines starting and ending at the same vertex).

The linked cluster expansion is based solely on graphs without self-loops, and therefore contributing graphs may be represented by a $V \times V$ symmetric matrix. The entries $A(i, j)$

of this so-called *incidence matrix* give the number of internal lines from v_i to v_j for $i \neq j$, and $A(i, i) = E(v_i)$ otherwise. The incidence matrices of topologically equivalent graphs are related through a permutation of the vertex labelling $(1, \dots, V)$. To eliminate multiple occurrences of equivalent graphs in the expansion, one has to define a certain canonical ordering of the vertices which must depend only on the topology of the graph under consideration. As a result, every equivalence class of graphs is represented by a single incidence matrix $A(i, j)$.

With each graph in the expansion one associates certain characteristic numbers which may depend on three sources: the topology of the graph, the underlying lattice structure or the local potential in the action.

The potential $u(\phi)$ only enters through the following weight factors. For a graph G with a set of vertices $\mathcal{V} = (v_1, \dots, v_V)$ it is defined as

$$\overset{\circ}{W}(G) = \prod_{v \in \mathcal{V}} \overset{\circ}{m}_{N(v)}^{\text{conn}}, \quad (53)$$

where the $\overset{\circ}{m}_{2k}^{\text{conn}}$ are the so-called connected moments. They can be calculated from the potential as follows.

The Taylor expansion of the free energy $W[J, K; \kappa]$ at zero coupling where all spins are uncorrelated and essentially randomly distributed can be written in terms of the so-called *cumulants* $\overset{\circ}{M}_k^{a_1 \dots a_k}(x_1)$ defined via

$$\left. \frac{\partial^k W}{\partial J^{a_1}(x_1) \dots \partial J^{a_k}(x_k)} \right|_{\kappa=0} = \delta(x_1, \dots, x_k) \overset{\circ}{M}_k^{a_1 \dots a_k}(x_1). \quad (54)$$

For zero external field, only the even correlation functions $W^{(2k, 0)}$ survive in a symmetric potential and the cumulants take a simple form

$$\begin{aligned} \left. \overset{\circ}{M}_{2k}^{a_1 \dots a_{2k}}(x_1) \right|_{J=K=0} &= \langle \phi^{a_1}(x_1) \dots \phi^{a_{2k}}(x_{2k}) \rangle^{\text{conn}} \Big|_{\kappa=0} \\ &= \delta(x_1, \dots, x_{2k}) \langle \phi^{a_1}(x_1) \dots \phi^{a_{2k}}(x_1) \rangle^{\text{conn}}, \end{aligned} \quad (55)$$

where the connected correlation functions are evaluated at one point in space-time and may be denoted by $\langle \phi^{a_1} \dots \phi^{a_{2k}} \rangle_1^{\text{conn}}$. From $O(N)$ invariance it follows that

$$\langle \phi^{a_1} \dots \phi^{a_{2k}} \rangle_1^{\text{conn}} = C_{2k}(a_1, \dots, a_{2k}) \overset{\circ}{m}_{2k}^{\text{conn}} \delta(x_1, \dots, x_{2k}), \quad (56)$$

where $\overset{\circ}{m}_{2k}^{\text{conn}}$ are the *connected moments* appearing in (53). The $C_{2k}(a_1, \dots, a_{2k})$ are $O(N)$ invariant tensors. The connected moments can easily be calculated from the (not necessarily connected) moments, which are defined in terms of the correlation functions

$$\langle \phi^{a_1} \dots \phi^{a_{2k}} \rangle_1 = C_{2k}(a_1, \dots, a_{2k}) \overset{\circ}{m}_{2k}. \quad (57)$$

Using the proper normalization condition for the $O(N)$ tensors one derives

$$\overset{\circ}{m}_{2k} = \frac{\Gamma(\frac{1}{2}N)}{2^k \Gamma(\frac{1}{2}N + k)} \frac{J_{N-1+2k}}{J_{N-1}}, \quad (58)$$

with

$$J_l = \int_0^\infty dr r^l \exp(-u(r)) . \quad (59)$$

In the limit $\lambda \rightarrow \infty$, the moments can be written as a ratio of polynomials in N . One has $\exp(-u(\phi)) \propto \delta(\phi^2 - 1)$ which results in $J_l = \text{const.}$ and thus

$$\mathring{m}_{2k} = \frac{1}{(N + 2k - 2)(N + 2k - 4) \dots (N + 2)N} . \quad (60)$$

From the moments the connected moments are generated via the relation

$$\sum_{k=1}^{\infty} \mathring{m}_{2k}^{\text{conn}} \frac{z^k}{k!} = \ln \left\{ 1 + \sum_{k=1}^{\infty} \mathring{m}_{2k} \frac{z^k}{k!} \right\} . \quad (61)$$

This concludes the calculation of the weight factors.

Next, with every graph G , one defines an internal symmetry number $S(G)$ as

$$S(G) = S_\pi(A) \prod_{i < j} A(i, j)! , \quad (62)$$

where $S_\pi(A)$ is the number of permutations that leave the incidence matrix invariant and the product represents the internal line multiplicity factor. A modified symmetry number $S_E(G)$ is defined which additionally takes the external line multiplicity into account by setting $i \leq j$ in the above expression.

The underlying lattice structure enters through the lattice embedding number $I(G)$ which counts the number of embeddings of G on the lattice under these conditions: the first vertex in G is fixed at the origin of the lattice and all other vertices are then distributed in such a way that any two vertices with distance 1 are placed on nearest neighbor lattice sites. Different vertices may be placed on the same site and different lines may occupy the same lattice link. Not all graphs are possible on a certain lattice structure. For example, graphs containing odd loops cannot be embedded on a hypercubic lattice. Note that for the susceptibility μ_2 , one has to introduce a modified lattice embedding number $I_2(G)$ which takes into account the additional factors of x^2 .

Finally, one defines a symmetry number associated with the internal $O(N)$ symmetry. For a graph G with a set of internal lines $\mathcal{L} = (l_1, \dots, l_L)$ one writes down an $O(N)$ index $a_l \in \{1, 2, \dots, N\}$ for every line l . Let $\{i_1, i_2, \dots, i_{I(v_i)}\}$ be the set of indices labelling the internal lines which terminate in vertex v_i . Then the $O(N)$ factor for G is given by

$$C(G) = \sum_{a_1, \dots, a_L=1}^N \prod_{i=1}^V C_{N(v_i)}(\underbrace{1, 1, \dots, 1}_{E(v_i) \text{ times}}, a_{i_1}, a_{i_2}, \dots, a_{i_{I(v_i)}}) . \quad (63)$$

$C(G)$ is a polynomial in N with maximum degree $\frac{1}{2}L$.

Having defined all the basic ingredients, one may now write down the unrenormalized expansion for the susceptibilities based on all equivalence classes of connected graphs without self-loops and with $N(v)$ even for all $v \in \mathcal{V}$ and $E = 2k$. These graphs are called \mathcal{G}_{2k} graphs

and the expansion reads

$$\chi_2 = \sum_{G \in \mathcal{G}_2} (2\kappa)^L I(G) C(G) \overset{\circ}{W}(G) \frac{E!}{S_E(G)} , \quad (64)$$

$$\mu_2 = \sum_{G \in \mathcal{G}_2} (2\kappa)^L I_2(G) C(G) \overset{\circ}{W}(G) \frac{E!}{S_E(G)} , \quad (65)$$

$$\chi_4 = \sum_{G \in \mathcal{G}_4} (2\kappa)^L I(G) C(G) \overset{\circ}{W}(G) \frac{E!}{S_E(G)} . \quad (66)$$

It can be recast in the form

$$\chi_2 = \sum_{L=0}^{\infty} \chi_2^{(L)} \frac{(2\kappa)^L}{L!} , \quad (67)$$

$$\mu_2 = \sum_{L=0}^{\infty} \mu_2^{(L)} \frac{(2\kappa)^L}{L!} , \quad (68)$$

$$\chi_4 = \sum_{L=0}^{\infty} \chi_4^{(L)} \frac{(2\kappa)^L}{L!} , \quad (69)$$

where the coefficients $\chi_2^{(L)}$, $\mu_2^{(L)}$ and $\chi_4^{(L)}$ are of the form

$$p[N] \prod_{k=1}^{\infty} (\overset{\circ}{m}_{2k}^{\text{conn}})^{n_k} , \quad (70)$$

with $\sum_{k=1}^{\infty} k n_k = L + \frac{1}{2}E$. The $p[N]$ are polynomials in N of order not higher than $\frac{1}{2}L$.

In order to reduce the total number of graphs, two levels of renormalization are carried out. A reduction in the number of contributing diagrams in the expansion is paid for with an increase in algebraic complexity.

The first step is to eliminate one-particle reducible graphs. A graph $G \in \mathcal{G}_{2k}$ is called *one-particle irreducible*, or 1PI, if it cannot be broken into two disconnected parts by cutting a single internal line. The set of 1PI graphs is denoted by \mathcal{G}_{2k}^{1PI} . The expansion over \mathcal{G}_{2k} can be reconstructed via

$$\chi_2 = \chi_2^{1PI} (1 - \epsilon \chi_2^{1PI})^{-1} , \quad (71)$$

$$\mu_2 = \left[\mu_2^{1PI} + \epsilon (\chi_2^{1PI})^2 \right] (1 - \epsilon \chi_2^{1PI})^{-2} , \quad (72)$$

$$\chi_4 = \chi_4^{1PI} (1 - \epsilon \chi_2^{1PI})^{-4} , \quad (73)$$

where χ_2^{1PI} , μ_2^{1PI} and χ_4^{1PI} stand for the 1PI part of the corresponding reducible quantities and $\epsilon = q2\kappa$. Here q is the coordination number of the lattice.

In a second step, one throws out one-vertex reducible graphs. A graph $G \in \mathcal{G}_{2k}^{1PI}$ is called *one-vertex irreducible*, or 1VI, if — after removal of any vertex and all the lines emanating from it — each remaining connected piece of G contains at least one external line. The set of 1VI graphs is denoted by \mathcal{S}_{2k} . Given the set \mathcal{S}_{2k} , the set \mathcal{G}_{2k}^{1PI} can be reconstructed by

attaching \mathcal{S}_{2k} graphs repeatedly to all $G \in \mathcal{S}_{2k}$ in a certain manner which I will not describe here. Furthermore, the connected moments $\overset{\circ}{m}_{2k}$ for the \mathcal{S}_{2k} graphs have to be redefined as

$$m_{2k} = \frac{1}{(2k-1)!!} \sum_{G \in \mathcal{P}_{2k}} (2\kappa)^L I(G) C(G) \overset{\circ}{W}(G) \frac{1}{S(G)}. \quad (74)$$

The m_{2k} are called *renormalized moments* and are evaluated over the set \mathcal{P}_{2k} , which is given by all graphs $G \in \mathcal{G}_{2k}$ with the additional constraint that all $2k$ external lines are attached to a single vertex. To lowest order one has $m_{2k} = \overset{\circ}{m}_{2k} + O(\kappa^2)$. The structure for the moments is the same as for the susceptibilities above. One finally has

$$\chi_2^{1PI} = \sum_{G \in \mathcal{S}_2} (2\kappa)^L I(G) C(G) W(G) \frac{E!}{S_E(G)}, \quad (75)$$

$$\mu_2^{1PI} = \sum_{G \in \mathcal{S}_2} (2\kappa)^L I_2(G) C(G) W(G) \frac{E!}{S_E(G)}, \quad (76)$$

$$\chi_4^{1PI} = \sum_{G \in \mathcal{S}_4} (2\kappa)^L I(G) C(G) W(G) \frac{E!}{S_E(G)}. \quad (77)$$

I will not go into details of the coding; the interested reader is referred to [2] and [15]. I will only give a brief outline and stress the differences to the hypercubic case.

To construct the set of \mathcal{S}_{2k} graphs required for the 1PI susceptibilities, I start out with a set of 'simple' graphs which will be expanded into the full set by a couple of basic operations. Let \mathcal{C}_1 be the set of simple and connected graphs without external lines which are 1PI and non-separable. As external lines are absent, non-separability is equivalent to one-vertex irreducibility. I denote the subset of \mathcal{C}_1 graphs with L internal lines by $\mathcal{C}_1(L)$. All the $\mathcal{C}_1(L)$ graphs can now be constructed by repeatedly applying two simple operations to the triangular graph, $C_1(3)$, represented by

$$\begin{pmatrix} 0 & 1 & 1 \\ 1 & 0 & 1 \\ 1 & 1 & 0 \end{pmatrix}.$$

(The zeroth order graph has to be added by hand.) All higher order graphs can then be generated

- by adding a single line between any two vertices with $A(i, j) = 0$, and
- by replacing a line by a bridge: a new graph is generated by removal of a line, say from v_i to v_j and addition of a new vertex w which is connected to both, v_i and v_j , by a single line each. The number of lines and the number of vertices is thus increased by one.

It is obvious that the resulting graphs are still simple and connected. However, the same graph may be constructed more than once. On the other hand no graph in \mathcal{C}_1 is left out, as any graph may always be reduced to the basic third order graph by simply applying the inverse operations. On a hypercubic lattice, graphs with odd loops are ruled out and one

would therefore start with the fourth order square graph. In this case it is convenient to modify the rules of construction such that graphs with zero lattice embedding number are not constructed at all. The number of $\mathcal{C}_1(L)$ graphs up to 13th order is given in table 1 for the general (i.e. F_4) case and for the hypercubic lattice.

To construct the set \mathcal{S}_{2k} from the set \mathcal{C}_1 , two additional conditions have to be satisfied. The total number of lines attached to each vertex $N(v)$ has to be even, and the number of external lines has to be $2k$. For the graph to be 1VI, at least two vertices must have external lines. Besides adding external and multiple internal lines to fulfill these conditions, the resulting graphs need to be coupled to generate the complete set of \mathcal{S}_{2k} graphs which are not necessarily non-separable but only 1VI. Details are given in [15]. The number of \mathcal{S}_{2k} for $k = 1, 2$ is also shown in table 1.

The total number of graphs generated up to 13th order is about 400,000. With 32 bit precision, this would require $\frac{1}{2} \cdot 13 \cdot 14 \cdot 4 \cdot 10^5 \cdot 4$ bytes = 145.6 Mb of storage on the computer. However, the incidence matrices can be stored in compressed form. Each matrix element requires a maximum of 4 bits at 13th order. Thus 12 4-byte integers are sufficient to represent a single matrix. A subset of graphs is simple and can be represented by just 3 integers. The total storage is therefore less than 19.2Mb.

The internal symmetry numbers and the $O(N)$ symmetry numbers are independent of the lattice structure and are calculated just as in the hypercubic case. For a detailed description of the procedure see [2]. The lattice embedding numbers are more involved and depend on the choice of lattice. They are calculated for a subset of so-called reduced graphs in order to minimize the calculational effort. There is a total of 6180 of these graphs up to 13th order, as compared with a total of 396,140 \mathcal{S}_{2k} graphs ($k = 1, 2$). The evaluation of the embedding number involves the number of random walks $\mathcal{N}_l[x]$ from the lattice origin to x in l steps. Instead of using a combinatorial approach to calculate these numbers, they are computed by actually carrying out the random walks on the lattice and creating a look-up table. This method can be adapted for different lattice structures without much effort. For the modified lattice embedding numbers each contribution is multiplied by an additional factor of $(x(i) - x(j))^2$, where v_i and v_j are the vertices with external lines. Factors of $\sqrt{2}$ enter on the F_4 lattice due to the length of basis vectors.

The renormalized moments are evaluated as in (74) over the set \mathcal{P}_{2k} which unfortunately is one-vertex reducible and therefore quite large. By introducing yet another set of 1VI graphs and new moments associated with these, it is possible to compute the renormalized moments order by order in terms of the new moments in a recursive manner. Consider a graph $G \in \mathcal{G}_2$ with $E(w) = 2$ and $I(w) = 2k$ for some vertex w . Now construct a new graph G' by removing the vertex w plus both its external lines. Note that G' is not necessarily connected nor 1PI or 1VI. One then defines

$$\mathcal{Q}_{2k} = \{G \in \mathcal{G}_2 | G' \text{ connected and 1VI} \} . \quad (78)$$

G' does not need to be 1PI. By construction, all graphs in $\mathcal{Q}_{2k}(L)$ will satisfy $L \geq 2k$. Observe that for G' to be one-vertex irreducible, all spikes must end in an external line. All external lines must have been connected to the vertex w before its removal. Therefore, G will consist of loops only. This in turn means that all \mathcal{Q}_{2k} graphs will in fact be 1PI. For a hypercubic lattice, all loops have an even number of lines and since $N(v)$ is even,

Table 1: Number of graphs contributing to \mathcal{C}_1 , \mathcal{S}_2 , \mathcal{S}_4 and \mathcal{Q}_{2k} . The second row gives the number of graphs that can be embedded on a hypercubic lattice. The numbers for \mathcal{Q}_{2k} are the sum of all contributing graphs, $k = 1, \dots, \infty$, at the given order.

L	\mathcal{C}_1	\mathcal{S}_2	\mathcal{S}_4	\mathcal{Q}_{2k}
0	1	1	1	0
	1	1	1	0
1	0	0	0	0
	0	0	0	0
2	0	0	1	1
	0	0	1	1
3	1	1	2	1
	0	1	1	0
4	1	1	6	2
	1	0	4	2
5	2	4	13	3
	0	2	4	0
6	4	8	44	7
	2	3	20	4
7	7	22	120	16
	1	8	27	0
8	16	57	416	41
	4	9	117	19
9	42	184	1364	106
	5	40	214	0
10	111	559	4935	309
	14	68	815	80
11	331	1910	17952	932
	20	247	1830	0
12	1098	6580	68774	2995
	65	470	6721	509
13	3829	24046	268524	9972
	124	1779	17028	0

L	\mathcal{S}_2	\mathcal{S}_4
0		
2		
3		
4		
5		

Figure 1: The contributions to \mathcal{S}_2 and \mathcal{S}_4 up to 5th order.

too, the graphs G , as well as G' must be of even order. This condition does not necessarily hold on other lattices, though, and in particular it is not true on an F_4 lattice. Finally, the new moments are evaluated in terms of the $\mathcal{Q}_{2k}(L)$ graphs and these are related to the renormalized moments in a recursive manner. Again, the full procedure is described in detail in [2].

With the renormalized moments, I have all the necessary components to evaluate the one particle irreducible parts of the susceptibilities as given in eqs. (75)—(77). After a simple re-expansion of the series, I obtain the final answer in the form of eqs. (67)—(69). Limited by computational resources, I carry out the expansion up to 13th order. On a hypercubic lattice, where the number of graphs is significantly fewer, Lüscher and Weisz were able to go to 14th order.

The total number of contributing terms in the expansion for $L \leq 13$ on the F_4 lattice is 387 for χ_2 , 357 for μ_2 , and 562 for χ_4 . The coefficients are given in tables 2—4 for the non-linear limit. For general λ , the coefficients are defined in terms of polynomials $p[N]$ multiplied by powers of the connected moments, see eq. (70). These numbers can be obtained from the author by electronic mail.

As a check on the computer program, I reproduce the high-temperature expansion up to 14th order on a hypercubic lattice. I am in full agreement with Lüscher and Weisz [2]. I also check the expansion on an F_3 (or *fcc*) lattice, where most previous data is for the Ising model. For χ_2 , I find agreement up to $L = 12$ with Gaunt, Sykes et. al [18]. For both, χ_2 and μ_2 , I agree with the data in the Baker-Kincaid tables [19] for the $N = 1$ case up to 10th order. My results are also in agreement with the data by Moore for the Ising model on an F_4 (or *hfcc*) lattice up to 10th order [20]. For μ_2 , however, I disagree at 10th order in the 14th digit. Since my $d = 3$ results for μ_2 agree with Baker-Kincaid at that order, and the $d = 4$ case is just a trivial extension, I am confident that my results are correct.

4 The triviality bound

From the high-temperature expansion the relevant physical quantities are calculated following Lüscher and Weisz [3, 4, 5]. Some modifications are necessary for the F_4 lattice. In the following analysis I will only consider the physical four component case. The evaluation of the series is improved by taking into account the scaling laws quoted in section 2. The results from the high-temperature expansion in the symmetric phase are being used as initial data to perform an integration of the RG equations towards the critical line. By matching the scaling behavior of the renormalized coupling, the integration is then continued into the broken phase up to $m_R = 0.5$. Finally, the result for m_R/f_π is compared with Monte Carlo data.

4.1 High-temperature series analysis in the symmetric phase

Approaching the second order critical line $\kappa_c(\lambda)$, the correlation length diverges — i.e. $\Lambda/m_R \rightarrow \infty$. In this limit, the theory is expected to behave like an effective, low-energy continuum theory. As one wants to obtain an upper bound on Λ/m_R at fixed renormalized coupling g_R (i.e. fixed physics) one has to minimize the function $m_R(\lambda)$ along the lines of

Table 2: Coefficients $\chi_2^{(L)}$ for $d = 4$, $\lambda = \infty$ and $N = 4$ on an F_4 lattice.

L	$\chi_2^{(L)}$
0	1 / 4
1	3 / 2
2	69 / 4
3	4 683 / 16
4	104 997 / 16
5	11 706 495 / 64
6	780 269 025 / 128
7	121 035 719 763 / 512
8	2 676 992 132 031 / 256
9	532 080 140 502 519 / 1 024
10	58 684 317 905 928 645 / 2 048
11	14 225 715 177 264 006 075 / 8 192
12	939 747 792 650 917 978 629 / 8 192
13	268 832 928 296 330 696 560 119 / 32 768

Table 3: Coefficients $\mu_2^{(L)}$ for $d = 4$, $\lambda = \infty$ and $N = 4$ on an F_4 lattice.

L	$\mu_2^{(L)}$
0	0
1	3 / 2
2	36 / 1
3	15 123 / 16
4	57 933 / 2
5	65 934 375 / 64
6	1 341 697 815 / 32
7	986 124 354 243 / 512
8	197 363 925 717 / 2
9	5 716 858 384 704 159 / 1 024
10	177 046 968 775 629 015 / 512
11	190 703 768 006 610 184 755 / 8 192
12	1 733 424 402 960 454 006 143 / 1 024
13	4 333 450 646 045 939 997 909 759 / 32 768

constant g_R (the RG trajectories). Thus, the first step is to compute the functions $m_R(\kappa, \lambda)$ and $g_R(\kappa, \lambda)$ from the high-temperature series.

The procedure is as follows. First I will determine the critical line $\kappa_c(\lambda)$. To identify possible additional singularities I apply the Padé approximant method. (Remember that on the F_4 lattice there is no simple anti-ferromagnetic singularity at $\kappa = -\kappa_c$.) Closer to the critical line, convergence of the series expansion becomes rather slow. However, LW found that the rate of convergence is “acceptable” as long as the correlation length does not exceed the average size (as measured in lattice spacings) of the graphs contributing to the cluster expansion. I choose as limit $m_R = 0.20$. In terms of κ , this condition is always satisfied in the region $\kappa \leq 0.98\kappa_c$. To obtain results in the region above $0.98\kappa_c$, I integrate the RG equations (again at fixed λ). The starting point for the integration is taken at the boundary line $\kappa = 0.98\kappa_c$. As g_R is driven towards zero at the transition, the perturbative expansions of the RG functions remain valid — provided the coupling is weak enough at the boundary line. A crude estimate of the applicability of renormalized perturbation theory is given by the tree-level unitarity bound on the renormalized coupling.

At this point let me recall that the results from the high-temperature expansion are for the susceptibilities χ_2 , μ_2 and χ_4 as in eqs. (46)—(48). From these, m_R , g_R , Z_R , and $Z_R^{\mathcal{O}}$ can be computed via eqs. (49)—(52). For the analysis, I switch to a new bare coupling $\bar{\lambda}$ which is defined in terms of the connected moments $\mathring{m}_{2k}^{\text{conn}}$ (see eq. (56)) as

$$\bar{\lambda} = -(1 + \frac{N}{2}) \mathring{m}_4^{\text{conn}} / (\mathring{m}_2^{\text{conn}})^2 . \quad (79)$$

It runs monotonically from 0 to 1. See table 5 for some values.

The convergence properties of the high-temperature expansion have been found to improve by reexpanding the series in powers of a so-called character variable v [3]. It can be expressed as

$$v = \frac{\sum_{l=1,3,5,\dots} \frac{1}{l!} (2\kappa)^l \frac{\Gamma(\frac{l+2}{2})}{\Gamma(\frac{N+l+1}{2})} J_{N+l}^2}{\sum_{l=0,2,4,\dots} \frac{1}{l!} (2\kappa)^l \frac{\Gamma(\frac{l+1}{2})}{\Gamma(\frac{N+l}{2})} J_{N+l-1}^2} . \quad (80)$$

In the Ising limit this reduces to the well known transformation $v = \tanh 2\kappa$. $\kappa_c(\lambda)$ is given by the pole in the series expansion of the susceptibility χ_2 and is extracted using the ratio method. Because all coefficients in the expansion $\chi_2 = \sum_{i=0}^{\infty} \chi_2^{(i)} v^i$ are positive, the pole closest to the origin must be on the positive real axis. This implies that the singularity is given by $v_c = \lim_{i \rightarrow \infty} r_i$ with $r_i = \chi_2^{(i-1)} / \chi_2^{(i)}$. For $i = 13$, the ratios have already converged rather well.

Based on the knowledge about the scaling behavior of the physical singularity in χ_2 , the extrapolation $i \rightarrow \infty$ can be improved. This behavior is described by eq. (35) and can be simulated by an auxiliary function of the form

$$\begin{aligned} h(z) &= (1-z)^{-1} \left(1 - f(\lambda) \ln(1-z) \right)^{-\delta_1/\beta_1} \\ &= \sum_{i=0}^{\infty} h^{(i)} z^i , \end{aligned} \quad (81)$$

Table 4: Coefficients $\chi_4^{(L)}$ for $d = 4$, $\lambda = \infty$ and $N = 4$ on an F_4 lattice.

L	$\chi_4^{(L)}$
0	-1 / 16
1	-3 / 2
2	-351 / 8
3	-6 069 / 4
4	-60 615 / 1
5	-175 900 185 / 64
6	-17 853 643 803 / 128
7	-2 005 549 316 799 / 256
8	-247 046 916 740 785 / 512
9	-33 114 590 817 471 513 / 1 024
10	-2 399 323 389 666 667 245 / 1 024
11	-747 560 932 086 148 219 743 / 4 096
12	-249 187 027 625 458 317 283 449 / 16 384
13	-44 243 685 707 698 463 691 882 177 / 32 768

Table 5: Values for κ_c and λ at given $\bar{\lambda}$. κ_c^P is from the Padé approximant, κ_c is from the extrapolation of the ratios.

$\bar{\lambda}$	λ	κ_c^P	κ_c
0.00	0.00	0.041667(1)	0.041666(1)
0.01	$0.1723 \cdot 10^{-2}$	0.041994(1)	0.041997(2)
0.02	$0.3566 \cdot 10^{-2}$	0.042332(2)	0.042339(3)
0.03	$0.5535 \cdot 10^{-2}$	0.042680(2)	0.042691(5)
0.04	$0.7639 \cdot 10^{-2}$	0.043041(3)	0.043054(6)
0.05	$0.9889 \cdot 10^{-2}$	0.043413(5)	0.043429(8)
0.06	$0.1229 \cdot 10^{-1}$	0.043797(5)	0.043815(9)
0.07	$0.1487 \cdot 10^{-1}$	0.044193(5)	0.04421(1)
0.08	$0.1762 \cdot 10^{-1}$	0.044602(6)	0.04462(1)
0.09	$0.2056 \cdot 10^{-1}$	0.045024(7)	0.04505(1)
0.10	$0.2370 \cdot 10^{-1}$	0.045459(7)	0.04549(1)
0.20	$0.7041 \cdot 10^{-1}$	0.05061(1)	0.05064(3)
0.30	0.1635	0.05728(1)	0.05732(4)
0.40	0.3451	0.06514(1)	0.06518(4)
0.50	0.6791	0.07314(2)	0.07317(5)
0.60	1.256	0.08004(4)	0.08005(6)
0.70	2.244	0.08514(6)	0.08517(6)
0.80	4.127	0.08849(6)	0.08851(6)
0.90	9.347	0.09044(8)	0.09045(5)
1.00	∞	0.0916(1)	0.09155(5)

where $f(\lambda)$ is given in eq. (36). Taking the ratios $r'_i = h^{(i-1)}/h^{(i)}$, one would expect similar convergence properties for r_i and r'_i . These two sequences are then combined to form a ratio $R_i = r_i/r'_i$, which somewhat stabilizes the series (especially closer to the non-linear limit). The value for v_c is obtained by fitting the monotonic fall-off in R_i to a $1/i^2$ form. The error Δv_c is taken as $\frac{1}{2}|R_{13} - v_c|$.

To study the distribution of singularities of χ_2 in the complex plane I use the Padé approximant method. Suppose the singularity of $f(z)$ can be written in the form $f(z) = A(z - z_c)^\alpha \{1 + \mathcal{O}(z - z_c)\}$ for $z \approx z_c$. Then the logarithmic derivative of $f(z)$ exhibits a simple pole at $z = z_c$ which is extracted using the Padé approximant. The exponent α is given by the residue at the pole.

Results for κ_c from both methods at selected values of $\bar{\lambda}$ are displayed in table 5. Notice that the values for κ_c from the Padé approximation are consistently below the result from the extrapolation of the ratios R_i . The difference is largest for intermediate $\bar{\lambda}$ where the first order scaling law improvement may not be adequate. On the other hand, the Padé method completely ignores the additional information about the nature of the physical poles gained from the scaling laws. Furthermore, the error estimation for κ_c^P is somewhat unclear and it is therefore difficult to draw definite conclusions. I will thus consider the results from the ratio method superior and use them throughout.

At $\lambda = \infty$, the critical point is $\kappa_c = 0.09155(5)$ which agrees with previous Monte Carlo data, $\kappa_c^{MC} = 0.0917(2)$ [13]. Except for the pole at κ_c^P , the Padé approximants only give spurious zeros or poles far away from the origin. Almost all of the roots in the polynomial $d(z)$ are on or very close to the real axis. The value for α from the Padé approximant is close to -1, as expected.

The calculation of the renormalized quantities m_R , g_R , Z_R , and $Z_R^{\mathcal{O}}$ is carried out along the boundary line $\kappa = 0.98\kappa_c$. From the scaling laws eqs. (29)–(32), the expansions can be written as

$$m_R = \left(1 - \frac{v}{v_c}\right)^{1/2} v^{-1/2} \hat{m}_R(v), \quad (82)$$

$$g_R = v^{-2} \hat{g}_R(v), \quad (83)$$

$$Z_R = v^{-1} \hat{Z}_R(v), \quad (84)$$

$$Z_R^{\mathcal{O}} = \hat{Z}_R^{\mathcal{O}}(v), \quad (85)$$

with the reduced expansion $\hat{m}_R(v) = \sum_{i=0}^{\infty} \hat{m}_R^{(i)} v^i$ and similarly for the other quantities. The scaling behavior of the reduced expansions can then be described by

$$\hat{m}_R(v) \propto \left(1 - f(\lambda) \ln\left(1 - \frac{v}{v_c}\right)\right)^{\delta_1/2\beta_1} (1 + \mathcal{O}(g_R \ln g_R)), \quad (86)$$

$$\hat{g}_R(v) \propto \left(1 - f(\lambda) \ln\left(1 - \frac{v}{v_c}\right)\right)^{-1} (1 + \mathcal{O}(g_R \ln g_R)), \quad (87)$$

$$\hat{Z}_R(v) \propto C(1 + \mathcal{O}(g_R \ln g_R)), \quad (88)$$

$$\hat{Z}_R^{\mathcal{O}}(v) \propto \left(1 - f(\lambda) \ln\left(1 - \frac{v}{v_c}\right)\right)^{-\delta_1/\beta_1} (1 + \mathcal{O}(g_R \ln g_R)), \quad (89)$$

which includes improvement. For the purpose of extrapolation and error estimation, auxiliary functions similar to eq. (82) are being introduced (except in the case of $\hat{Z}_R(v)$, which tends to

a constant). From the overlap of the reduced expansion with the auxiliary function one can extract the extrapolated value as well as a reliable error estimate. In fact, the proportionality factor $C = v_c^i \hat{m}_R^{(i)} / h^{(i)}$ is monotonic and stabilizes for $i \geq 10$. With the high-temperature expansion up to 13th order, the remainder of the series can be reliably estimated as

$$\delta = C \left\{ h(z) - \sum_{i=0}^{L-1} h^{(i)} z^i \right\}_{z=v/v_c}, \quad (90)$$

such that the extrapolated estimate for the (reduced) mass is given by

$$\hat{m}_R^*(v) = \sum_{i=0}^{L-1} \hat{m}_R^{(i)} v^i + \delta. \quad (91)$$

From the variation in the overlap I obtain an error on δ and thus on the mass m_R . The quantities g_R and $Z_R^{\mathcal{O}}$ are treated similarly. For Z_R , however, I evaluate $\hat{Z}_R(v)$ for $L, L-1, L-2, \dots$ and extract the best estimate by fitting the monotonic behavior of the truncated series to a quadratic fall-off in L .

Results for m_R , g_R , Z_R , and $Z_R^{\mathcal{O}}$ along the boundary line $\kappa = 0.98\kappa_c$ are given in table 6. All errors are within 2% and the maximal correlation length is less than 5, compatible with the demand that it be less than the average extent of the graphs in the linked cluster expansion. As expected, the maximal value for the coupling g_R along the boundary line occurs in the σ -model limit with $g_R = 15.8(2)$, about half the unitarity bound.

I compare the results from the 13th order calculation with those from the 12th order to check for inconsistencies in the error estimates. At 12th order, the critical line is shifted to slightly higher κ values, but always much less than one standard deviation. The change in κ_c has a negligible effect on m_R , g_r and $Z_R^{\mathcal{O}}$, the effect on Z_R , however, is noticeable, particularly for $\lambda \leq 0.1$. This indicates that the error for Z_R may be underestimated, but this will have no effect on the final result for the triviality bound.

As a further check, I evaluate the high-temperature series at $\kappa = 0.09$ in the σ -model limit (even though this point is slightly above the boundary line). Here, Monte Carlo data [13] predict $g_R = 15.5(1.5)$ and $m_R = 0.2075(15)$. I obtain $g_R = 15.2(3)$ and $m_R = 0.2054(2)$. The Monte Carlo mass is significantly heavier, maybe indicating slight contamination by excited states.

I now turn to the integration of the RG equations (22)–(25) in the region $0.98\kappa_c \leq \kappa \leq \kappa_c$ which is done numerically, starting from the results of the high-temperature series at the boundary line. The results are displayed in tables 7–9 for selected values of $\bar{\lambda}$ and in the range $0.01 \leq m_R \leq 1.0$. The values for $\kappa \leq 0.98\kappa_c$ are from the high-temperature series analysis. For the integration I use the RG functions up to three loops including the lattice dependent scaling violating terms up to 1-loop order. At this order, the scaling violations in the region $\kappa > 0.98\kappa_c$ are always less than 6% of the universal part. Therefore, the mass dependent terms are omitted at higher orders. From the tables notice that $\kappa \rightarrow \kappa_c$ as $m_R \rightarrow 0$, as it should be. Errors are estimated by propagating the errors of the initial data and do not include the systematic uncertainties due to the approximation of the RG functions. To estimate this systematics, I use the 2-loop approximations instead, and the effect for g_R in the non-linear limit is demonstrated in fig. 2. Generally, the difference between the 2-loop and 3-loop approximations is maximal in the non-linear limit.

Table 6: High-temperature expansion results for m_R , g_R , Z_R , and $Z_R^{\mathcal{O}}$ at $\kappa = 0.98\kappa_c$.

λ	κ	m_R	g_R	Z_R	$Z_R^{\mathcal{O}}$
0.00	0.0408333	0.285714(1)	0.0	4.0816326(3)	0.0102083(1)
0.01	0.0411575	0.28442(6)	0.32854(1)	4.049486(1)	0.010342(1)
0.02	0.0414919	0.2832(1)	0.64820(5)	4.016840(5)	0.010479(1)
0.03	0.0418369	0.2820(2)	0.9596(1)	3.98370(1)	0.010619(3)
0.04	0.0421929	0.2808(2)	1.2633(3)	3.95008(2)	0.010763(3)
0.05	0.0425601	0.2797(3)	1.5597(5)	3.91597(3)	0.010910(4)
0.06	0.0429388	0.2787(3)	1.8492(9)	3.88140(4)	0.011060(5)
0.07	0.0433295	0.2776(4)	2.132(1)	3.84637(5)	0.011215(6)
0.08	0.0437324	0.2766(4)	2.409(2)	3.81090(7)	0.011373(7)
0.09	0.0441479	0.2756(4)	2.680(2)	3.77500(8)	0.011535(8)
0.10	0.0445763	0.2747(5)	2.945(3)	3.7387(1)	0.011701(9)
0.20	0.0496317	0.2664(7)	5.33(1)	3.3573(3)	0.01362(2)
0.30	0.0561757	0.2595(8)	7.34(2)	2.9653(6)	0.01608(3)
0.40	0.0638780	0.2535(8)	9.05(3)	2.6068(9)	0.01904(4)
0.50	0.0717026	0.2480(7)	10.54(4)	2.321(1)	0.02221(5)
0.60	0.0784481	0.2429(7)	11.84(3)	2.120(1)	0.02523(6)
0.70	0.0834642	0.2381(6)	12.98(2)	1.992(2)	0.02784(6)
0.80	0.0867365	0.2335(5)	14.00(1)	1.915(2)	0.02999(6)
0.90	0.0886387	0.2291(4)	14.92(3)	1.872(2)	0.03175(5)
1.00	0.0897232	0.2248(2)	15.8(2)	1.848(3)	0.03331(3)

Table 7: Results in the symmetric phase at given m_R for $\bar{\lambda} = 0.01$. The values for $\kappa \leq 0.98\kappa_c(\bar{\lambda})$ are from the high-temperature expansion, while those for $\kappa > 0.98\kappa_c(\bar{\lambda})$ are from the integration of the RG equations.

λ	m_R	g_R	Z_R	Z_R^O	κ
0.01	1.00	0.4978807(2)	4.9641184(1)	0.00840706(1)	0.03357427(5)
	0.90	0.4604509(4)	4.7752191(2)	0.00874153(3)	0.03490241(8)
	0.80	0.4281371(7)	4.6061668(3)	0.00906474(5)	0.0361834(1)
	0.70	0.400522(1)	4.4569599(4)	0.00937124(9)	0.0373947(2)
	0.60	0.377231(2)	4.3275968(6)	0.0096553(2)	0.0385125(3)
	0.50	0.357933(3)	4.2180769(8)	0.0099111(3)	0.0395125(3)
	0.40	0.342329(5)	4.128401(1)	0.0101333(5)	0.0403707(4)
	0.30	0.330145(8)	4.058578(1)	0.0103173(8)	0.0410653(4)
	0.20	0.321093(9)	4.008676(1)	0.0104605(9)	0.041576(2)
	0.10	0.314617(9)	3.978685(1)	0.0105666(9)	0.041890(2)
	0.09	0.314058(8)	3.976782(1)	0.0105760(9)	0.041910(2)
	0.08	0.313500(8)	3.975078(1)	0.0105853(9)	0.041928(2)
	0.07	0.312937(8)	3.973574(1)	0.0105948(9)	0.041944(2)
	0.06	0.312355(8)	3.972270(1)	0.0106046(9)	0.041957(2)
	0.05	0.311736(8)	3.971165(1)	0.0106151(9)	0.041969(2)
	0.04	0.311051(8)	3.970260(1)	0.0106267(9)	0.041979(2)
	0.03	0.310243(8)	3.969555(1)	0.0106405(9)	0.041986(2)
	0.02	0.309185(8)	3.969050(1)	0.0106587(9)	0.041991(2)
	0.01	0.307477(8)	3.968744(1)	0.0106884(9)	0.041995(2)

Table 8: Same as table 7 but for $\bar{\lambda} = 0.1$.

λ	m_R	g_R	Z_R	$Z_R^{\mathcal{O}}$	κ
0.10	1.00	4.81569(7)	4.61008(1)	0.0091809(1)	0.0361520(4)
	0.90	4.4304(1)	4.43251(2)	0.0095684(3)	0.0376002(6)
	0.80	4.0942(2)	4.27330(2)	0.0099494(5)	0.039001(1)
	0.70	3.8021(4)	4.13246(4)	0.0103196(9)	0.040330(1)
	0.60	3.5497(6)	4.00996(5)	0.010675(2)	0.041562(2)
	0.50	3.332(1)	3.90583(6)	0.011011(3)	0.042669(3)
	0.40	3.146(2)	3.82007(8)	0.011328(5)	0.043627(3)
	0.30	2.983(3)	3.7528(1)	0.011627(8)	0.044409(3)
	0.20	2.833(3)	3.7043(1)	0.011926(9)	0.04499(1)
	0.10	2.666(3)	3.67481(9)	0.01229(1)	0.04535(1)
	0.09	2.645(2)	3.67290(9)	0.01234(1)	0.04537(1)
	0.08	2.623(2)	3.67117(9)	0.01239(1)	0.04539(1)
	0.07	2.599(2)	3.66963(9)	0.01245(1)	0.04541(1)
	0.06	2.572(2)	3.66829(9)	0.01251(1)	0.04543(1)
	0.05	2.541(2)	3.66712(9)	0.01259(1)	0.04544(1)
	0.04	2.505(2)	3.66615(9)	0.01268(1)	0.04545(1)
	0.03	2.461(2)	3.66535(9)	0.01280(1)	0.04546(1)
	0.02	2.402(2)	3.66472(9)	0.01296(1)	0.04547(1)
	0.01	2.307(2)	3.66421(9)	0.01322(1)	0.04547(1)

Table 9: Same as table 7 but for $\bar{\lambda} = 1.0$.

λ	m_R	g_R	Z_R	$Z_R^{\mathcal{O}}$	κ
1.00	1.00	40.241(3)	2.3957(2)	0.0200322(3)	0.0694724(2)
	0.90	36.014(6)	2.2927(3)	0.0212659(5)	0.0725736(4)
	0.80	32.22(1)	2.1991(5)	0.022583(1)	0.0756370(7)
	0.70	28.81(2)	2.1149(7)	0.023996(2)	0.078616(1)
	0.60	25.72(3)	2.040(1)	0.025525(4)	0.081454(2)
	0.50	22.88(6)	1.975(1)	0.027200(7)	0.084092(2)
	0.40	20.2(1)	1.920(2)	0.02908(1)	0.086459(3)
	0.30	17.7(2)	1.875(2)	0.03129(2)	0.088481(4)
	0.20	15.1(3)	1.841(3)	0.03408(4)	0.090073(3)
	0.10	12.1(1)	1.819(3)	0.0383(1)	0.09113(5)
	0.09	11.7(1)	1.818(3)	0.0389(1)	0.09121(5)
	0.08	11.3(1)	1.816(3)	0.0395(1)	0.09127(5)
	0.07	11.0(1)	1.815(3)	0.0402(1)	0.09133(5)
	0.06	10.5(1)	1.814(3)	0.0411(1)	0.09139(5)
	0.05	10.1(1)	1.812(3)	0.0420(1)	0.09143(5)
	0.04	9.59(9)	1.811(3)	0.0432(2)	0.09147(5)
	0.03	9.02(8)	1.810(3)	0.0446(2)	0.09150(5)
	0.02	8.31(7)	1.809(2)	0.0466(2)	0.09152(5)
	0.01	7.33(5)	1.808(2)	0.0498(3)	0.09154(5)

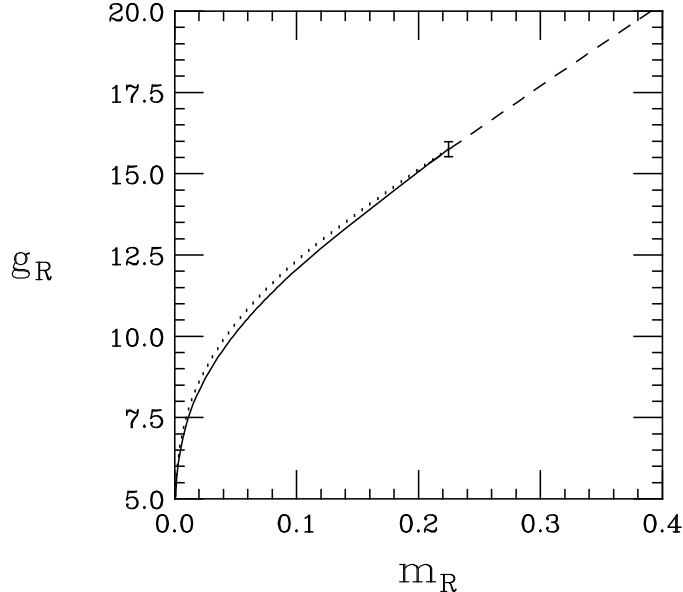


Figure 2: Comparison of the solutions of the RG equations at two and three loops for g_R at $\bar{\lambda} = 1$. The dashed line is the result from the high-temperature expansion, while the solid line is the continuation obtained by integrating the 3-loop approximation of the β -function. The dotted curve corresponds to the 2-loop approximation. It is evident that the deviations in the symmetric phase are of the same size as the series expansion error in g_R calculated at the boundary line.

4.2 Continuation of the analysis to the broken symmetry phase

As indicated in section 2, to continue the solution of the theory into the broken phase one needs to evaluate the integration constants C_1 , C_2 , and C_3 at the transition. These constants are defined through the scaling behavior of m_R , Z_R , and $Z_R^{\mathcal{O}}$ in eqs. (3), (26) and (27) and can be computed by numerically integrating the RG equations down to small m_R , for instance $m_R = 10^{-8}$, using the 3-loop expressions. In this region $\ln C_i$ is linear in g_R and the limit $g_R \rightarrow 0$ can be extracted. The results for some values of $\bar{\lambda}$ are presented in table 10.

Given the integration constants on the high-temperature side of the transition, the constants C'_i in the broken phase are fixed through eq. (45). m_R , Z_R , and $Z_R^{\mathcal{O}}$ can then be calculated using the broken phase scaling laws. I choose $g_R = 10^{-8}$ — small enough for order g_R^2 corrections to be negligible — and continue integrating the RG equations up to $m_R = 0.5$, again using the 3-loop expressions for the RG functions including scaling violating terms up to 1-loop. The results at $m_R = 0.5$ are displayed in table 11 for selected values of $\bar{\lambda}$. Results along the lines of constant $\bar{\lambda}$ are shown in tables 12–14. Errors are estimated by propagating the uncertainties in the integration constants only. The renormalized coupling is maximal in the non-linear limit where it reaches $g_R = 18(1)$ at $m_R = 0.5$, about 2/3 the unitarity bound. The assumption of applicability of perturbative RG is justified by comparing the 3-loop with the 2-loop results: the changes in the region $m_R \leq 0.5$ are not unreasonable.

In fig. 3 I compare the results for m_R/f_π with recent Monte Carlo data [13]. Both methods

Table 10: Values for $\ln C_i$ at the critical line.

λ	$\ln C_1$	$\ln C_2$	$\ln C_3$
0.01	126.429(4)	1.3782607(3)	-5.1270(1)
0.02	64.356(5)	1.370040(1)	-4.7730(2)
0.03	43.563(7)	1.361631(2)	-4.5625(3)
0.04	33.116(8)	1.353031(4)	-4.4106(5)
0.05	26.82(1)	1.344237(6)	-4.2907(6)
0.06	22.60(1)	1.335249(9)	-4.1909(7)
0.07	19.57(1)	1.32606(1)	-4.1049(9)
0.08	17.29(1)	1.31668(1)	-4.029(1)
0.09	15.51(1)	1.30710(2)	-3.961(1)
0.10	14.07(2)	1.29731(2)	-3.898(1)
0.20	7.50(2)	1.18865(8)	-3.441(3)
0.30	5.22(2)	1.0636(2)	-3.110(4)
0.40	4.04(2)	0.9340(3)	-2.831(4)
0.50	3.32(1)	0.8173(4)	-2.596(4)
0.60	2.82(1)	0.7263(6)	-2.407(4)
0.70	2.460(7)	0.6633(8)	-2.259(3)
0.80	2.184(4)	0.624(1)	-2.144(3)
0.90	1.963(7)	0.601(1)	-2.052(3)
1.00	1.78(4)	0.588(1)	-1.975(9)

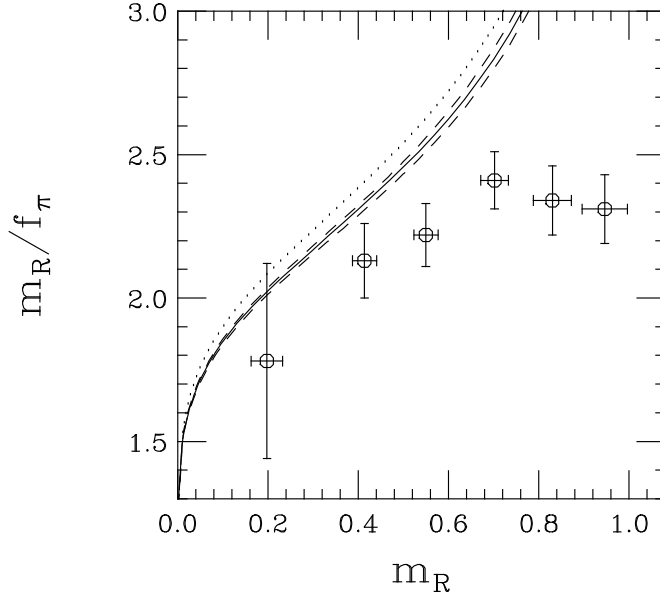


Figure 3: Ratio m_R/f_π versus m_R in lattice units. The solid line is from integrating the RG equations. The dashed line gives the propagated error and the dotted line is the 2-loop result. The data points are from a Monte Carlo simulation [13].

are in fair agreement for $m_R < 0.5$. For larger masses, however, one leaves the perturbative regime and the integration of the perturbative RG functions cannot be trusted anymore. Also, the $L \rightarrow \infty$ extrapolation of the Monte Carlo data may be spoiled by σ -particle decay, perhaps leading to the systematic difference evident in fig. 3. At $\Lambda/m_R = 2$ I obtain for an upper bound on the Higgs mass

$$m_R/f_\pi \leq 2.46 \pm 0.02_{\text{HTE}} \pm 0.08_{\text{PT}} , \quad (92)$$

where the first error is from the extrapolation of the high-temperature expansion and the second error is from the perturbative expansion of the RG functions. The latter is estimated by comparing the 2-loop and the 3-loop results. The above numbers translate to about $600 \pm 5_{\text{HTE}} \pm 20_{\text{PT}}$ GeV. The Monte Carlo result is $2.3(2)$ [13], somewhat below the number from the high-temperature expansion. The agreement is better in the second reference of [13], where in a similar plot the RG integration is based on Monte Carlo data in the symmetric phase. This indicates that the systematic difference in fig. 3 is mainly due to the expansion itself and not to the perturbative RG integration.

The F_4 results compare to $m_R/f_\pi \leq 2.6(3)$ (or $640(70)$ GeV) from the high-temperature expansion on a hypercubic lattice [9, 5]. Here Monte Carlo simulations give $2.7(1)$ [10], slightly *above* the semi-analytical result. Interestingly, the hypercubic results are in reverse order.

Even though the maximal cutoff on the F_4 lattice seems to be about 6% lower than LW's hypercubic result [4], this statement by itself is not meaningful. One must not directly compare the two cutoffs as they have different meanings on different lattices. This is evident in the lattice dependence of the scaling violations. Rather, one should consider the cutoff dependence of physical quantities, such as the pion—pion 90 degree scattering cross section.

Table 11: Results in the broken phase at $m_R = 0.5$ from integrating the RG equations.

λ	κ	g_R	Z_R	$Z_R^{\mathcal{O}}$
0.01	0.043384(1)	0.290944(8)	3.841565(1)	0.010567(1)
0.02	0.043739(3)	0.57660(5)	3.810283(4)	0.010709(3)
0.03	0.044106(4)	0.8573(1)	3.778535(9)	0.010855(4)
0.04	0.044484(5)	1.1335(3)	3.74633(2)	0.011004(6)
0.05	0.044874(6)	1.4053(5)	3.71368(2)	0.011156(8)
0.06	0.045276(8)	1.6731(8)	3.68059(3)	0.01131(1)
0.07	0.045691(9)	1.937(1)	3.64707(4)	0.01147(1)
0.08	0.04612(1)	2.197(2)	3.61313(6)	0.01164(2)
0.09	0.04656(1)	2.454(2)	3.57879(7)	0.01180(2)
0.10	0.04701(1)	2.708(3)	3.54407(8)	0.01198(2)
0.20	0.05238(2)	5.08(1)	3.1800(3)	0.01397(5)
0.30	0.05933(2)	7.21(3)	2.8068(5)	0.01652(9)
0.40	0.06752(3)	9.15(4)	2.4659(8)	0.0196(1)
0.50	0.07585(3)	10.92(4)	2.195(1)	0.0229(1)
0.60	0.08305(4)	12.55(4)	2.004(1)	0.0261(1)
0.70	0.08844(4)	14.05(3)	1.882(2)	0.0288(1)
0.80	0.09199(5)	15.46(2)	1.809(2)	0.0310(1)
0.90	0.09409(4)	16.79(4)	1.768(2)	0.0329(1)
1.00	0.09534(2)	18.1(3)	1.745(2)	0.0345(6)

Table 12: Results in the broken phase at given m_R for $\bar{\lambda} = 0.01$.

λ	m_R	g_R	Z_R	$Z_R^{\mathcal{O}}$	κ
0.01	0.01	0.306186(8)	3.967302(1)	0.010722(1)	0.041998(2)
	0.02	0.307806(8)	3.967149(1)	0.010693(1)	0.042000(2)
	0.03	0.308731(8)	3.966898(1)	0.010676(1)	0.042002(2)
	0.04	0.309357(8)	3.966549(1)	0.010664(1)	0.042006(2)
	0.05	0.309810(8)	3.966101(1)	0.010655(1)	0.042011(2)
	0.06	0.310147(8)	3.965555(1)	0.010647(1)	0.042017(2)
	0.07	0.310396(8)	3.964909(1)	0.010641(1)	0.042023(2)
	0.08	0.310576(8)	3.964165(1)	0.010635(1)	0.042031(2)
	0.09	0.310698(8)	3.963322(1)	0.010630(1)	0.042040(2)
	0.10	0.310770(8)	3.962380(1)	0.010626(1)	0.042051(2)
	0.20	0.309520(8)	3.947501(1)	0.010597(1)	0.042211(2)
	0.30	0.305563(8)	3.922586(1)	0.010580(1)	0.042481(2)
	0.40	0.299318(8)	3.887393(1)	0.010570(1)	0.042869(2)
	0.50	0.290944(8)	3.841565(1)	0.010567(1)	0.043384(1)

Table 13: Same as table 12 but for $\bar{\lambda} = 0.1$.

λ	m_R	g_R	Z_R	$Z_R^{\mathcal{O}}$	κ
0.10	0.01	2.237(2)	3.65503(9)	0.01354(2)	0.04549(1)
	0.02	2.325(2)	3.65471(9)	0.01328(2)	0.04549(1)
	0.03	2.380(2)	3.65437(9)	0.01312(2)	0.04549(1)
	0.04	2.420(2)	3.65397(9)	0.01301(2)	0.04550(1)
	0.05	2.453(2)	3.65349(9)	0.01293(2)	0.04550(1)
	0.06	2.479(2)	3.65293(9)	0.01286(2)	0.04551(1)
	0.07	2.502(2)	3.65230(9)	0.01279(2)	0.04552(1)
	0.08	2.522(2)	3.65158(9)	0.01274(2)	0.04553(1)
	0.09	2.540(2)	3.65078(9)	0.01269(2)	0.04554(1)
	0.10	2.556(2)	3.64989(9)	0.01265(2)	0.04555(1)
	0.20	2.658(3)	3.63640(9)	0.01237(2)	0.04573(1)
	0.30	2.705(3)	3.61440(9)	0.01220(2)	0.04603(1)
	0.40	2.719(3)	3.58373(9)	0.01207(2)	0.04646(1)
	0.50	2.708(3)	3.54407(8)	0.01198(2)	0.04701(1)

Table 14: Same as table 12 but for $\bar{\lambda} = 1.0$.

λ	m_R	g_R	Z_R	$Z_R^{\mathcal{O}}$	κ
1.00	0.01	6.64(4)	1.793(2)	0.0538(7)	0.09156(5)
	0.02	7.43(5)	1.792(2)	0.0509(6)	0.09156(5)
	0.03	7.99(6)	1.792(2)	0.0491(6)	0.09158(5)
	0.04	8.43(7)	1.791(2)	0.0478(6)	0.09159(5)
	0.05	8.81(8)	1.790(2)	0.0468(6)	0.09161(5)
	0.06	9.14(8)	1.790(2)	0.0460(6)	0.09163(5)
	0.07	9.45(9)	1.789(2)	0.0452(6)	0.09166(5)
	0.08	9.73(9)	1.789(2)	0.0446(6)	0.09169(5)
	0.09	10.0(1)	1.788(2)	0.0440(6)	0.09172(5)
	0.10	10.2(1)	1.787(2)	0.0435(6)	0.09176(5)
	0.20	12.3(1)	1.780(2)	0.0400(6)	0.09230(4)
	0.30	14.1(2)	1.770(2)	0.0377(6)	0.09312(2)
	0.40	16.0(2)	1.758(2)	0.0360(6)	0.09415(2)
	0.50	18.1(3)	1.745(2)	0.0345(6)	0.09534(2)

By demanding that the deviation

$$\delta = \frac{(d\sigma/d\theta)^{\text{lattice}}}{(d\sigma/d\theta)^{\text{continuum}}} - 1 \quad (93)$$

be less than (say) 0.3% for all energies up to some center-of-mass energy, for instance up to $2m_R$, one defines a physically relevant bound. On the F_4 lattice, $\delta < 0.3\%$ translates to $m_R \approx 0.5$, whereas on the hypercubic lattice the same requirement gives $m_R \approx 0.22$ [12]. From [9], this value corresponds to $m_R/f_\pi = 2.2$ or roughly 540 GeV, which is actually about 10% below the F_4 bound.

To summarize, in the broken phase I find that for $\Lambda/m_R \geq 2$ the coupling never exceeds 2/3 of the triviality bound (as in the hypercubic case, see [5]), indicating that there is in fact not much room for a heavy Higgs — if one insists on keeping the naive lattice action. A Monte Carlo study including dimension six operators parameterizing the leading order (Λ^{-2}) cutoff effects has shown that the bound may be as high as 710(60) GeV [14]. A high-temperature expansion for the improved action case would be desirable but poses quite a complicated task.

Going from 12th to 13th order in the expansion quadruples the number of contributing graphs and one reaches the limits of today's computational resources. Furthermore, at this order, the uncertainty due to the perturbative RG functions is by far larger than the uncertainty due to the series expansion. Hence it does not pay to attempt a 14th order calculation without simultaneous improvement in the perturbative results for the RG functions.

Finally, I would like to remind the reader that the solution of the ϕ^4 theory as presented here rests on the assumption that perturbation theory can be applied for sufficiently small couplings (thereby implicitly assuming triviality), and relies on the fact that the perturbative region overlaps with the region in the symmetric phase where the linked cluster expansion can be evaluated. These issues are discussed in detail in LW's papers.

The advantages of the semi-analytical approach over Monte Carlo methods are evident: the lack of finite size effects and the absence of statistical errors. Furthermore, one does not have to worry about the σ -particle decay which complicates the extraction of m_σ on larger lattices in Monte Carlo simulations. However, with respect to fig. 3 it is not clear from which source the differences arise. All one can say is that the comparison gives a good estimate of systematic errors which are very different in both methods and presumably do not alter the results in the same direction.

Acknowledgements

I would like to thank my former advisor, Urs M. Heller for invaluable support. Thanks also go to Pavlos Vranas and Herbert Neuberger. This project was supported in part by the Department of Energy under contract number DE-FC05-85 ER250000 and the Supercomputer Computations Research Institute and The Florida State University Department of Physics through use of their facilities. The linked cluster expansion was performed on the cluster of IBM RS6000 workstations at SCRI. The final stage of this project was carried out while the author was at Columbia University, supported under contract number DE-FG02-92 ER40699.

Appendix

This appendix gives the (slightly corrected) coefficients for the RG function (cf. [5, 12]). Writing

$$\beta(0, g_R) = g_R \sum_{\nu=1}^{\infty} \beta_{\nu} g_R^{\nu}, \quad (94)$$

$$\gamma(0, g_R) = \sum_{\nu=1}^{\infty} \gamma_{\nu} g_R^{\nu}, \quad (95)$$

$$\delta(0, g_R) = \sum_{\nu=1}^{\infty} \delta_{\nu} g_R^{\nu}, \quad (96)$$

the universal coefficients are given by

$$\beta_1 = \frac{1}{3}(N+8)(16\pi^2)^{-1}, \quad (97)$$

$$\beta_2 = -\frac{1}{3}(3N+14)(16\pi^2)^{-2}, \quad (98)$$

$$\beta_3 = \frac{1}{432} \left\{ 61N^2 + 1782N + 5744 + 192\zeta(3)(5N+22) - 2k(N+8)(13N+62) \right\} (16\pi^2)^{-3}, \quad (99)$$

$$\gamma_1 = 0, \quad (100)$$

$$\gamma_2 = \frac{1}{36}(N+2)(16\pi^2)^{-2}, \quad (101)$$

$$\gamma_3 = -\frac{1}{432}(N+2)(N+8)(1-2k)(16\pi^2)^{-3}, \quad (102)$$

$$\delta_1 = -\frac{1}{3}(N+2)(16\pi^2)^{-1}, \quad (103)$$

$$\delta_2 = \frac{5}{18}(N+2)(16\pi^2)^{-2}, \quad (104)$$

$$\delta_3 = -\frac{1}{216}(N+2) \left\{ 31N + 221 + 6k(N+1) \right\} (16\pi^2)^{-3}, \quad (105)$$

where

$$k = 1.62520965, \quad (106)$$

$$\zeta(3) = 1.20205690, \quad (107)$$

the latter being the Riemann zeta function. The non-universal scaling violating terms up to one loop are

$$\beta(m_R, g_R) = g_R \sum_{\nu=0}^{\infty} u_{\nu}(m_R) g_R^{\nu}, \quad (108)$$

$$\gamma(m_R, g_R) = \sum_{\nu=0}^{\infty} v_{\nu}(m_R) g_R^{\nu}, \quad (109)$$

$$\delta(m_R, g_R) = \sum_{\nu=0}^{\infty} w_{\nu}(m_R) g_R^{\nu}, \quad (110)$$

with the coefficients

$$u_0 = \frac{4m_R^2}{4 + m_R^2}, \quad (111)$$

$$u_1 = \frac{1}{6}u_0 \left\{ (N+8)(4 + m_R^2)J_3(m_R^2) - 6J_2(m_R^2) - (N+2)\frac{1}{4 + m_R^2} J_1(m_R^2) \right\}, \quad (112)$$

$$v_0 = \frac{1}{4}u_0, \quad (113)$$

$$v_1 = \frac{1}{24}(N+2)u_0 \left\{ J_2(m_R^2) - \frac{1}{4 + m_R^2} J_1(m_R^2) \right\}, \quad (114)$$

$$w_0 = -\frac{1}{2}u_0, \quad (115)$$

$$w_1 = -2v_1 - \frac{1}{6}(N+2)m_R^2 \left\{ (4 + m_R^2)J_3(m_R^2) - 2J_2(m_R^2) + \frac{1}{4 + m_R^2} J_1(m_R^2) \right\}. \quad (116)$$

The lattice integrals $J_p(m_R^2)$ are defined as

$$J_p(m_R^2) = \int_k \frac{1}{[g(k) + m_R^2]^p} \quad (117)$$

and are evaluated numerically.

In the broken phase, the universal coefficients β_1 , β_2 , γ_1 , and δ_1 take the same form as in the symmetric phase; the differing coefficients are given by

$$\beta_3 = \left\{ -\frac{\pi^2}{108}N^3 - 0.6038002N^2 + 6.006124N + 11.10641 \right\} (16\pi^2)^{-3}, \quad (118)$$

$$\gamma_2 = -\frac{1}{6}(16\pi^2)^{-2}, \quad (119)$$

$$\gamma_3 = \left\{ -0.0452317896N + 0.211712032 \right\} (16\pi^2)^{-3}, \quad (120)$$

$$\delta_2 = \frac{1}{18} \left\{ (5 + 2\sqrt{3}\pi)N + 16 - 2\sqrt{3}\pi \right\} (16\pi^2)^{-2}, \quad (121)$$

$$\delta_3 = \left\{ \frac{\pi^2}{108}N^3 + 1.2932334N^2 - 4.320590N + 1.620019 \right\} (16\pi^2)^{-3}. \quad (122)$$

For the function ϵ , the power series is written as

$$\epsilon(0, g_R) = \sum_{\nu=0}^{\infty} \epsilon_{\nu} g_R^{\nu}, \quad (123)$$

with the universal coefficients

$$\epsilon_0 = 1, \quad (124)$$

$$\epsilon_0 = \frac{1}{6} \left\{ -N + 3 - 2\sqrt{3}\pi \right\} (16\pi^2)^{-1}, \quad (125)$$

$$\epsilon_0 = \left\{ 0.503662N + 2.487506 \right\} (16\pi^2)^{-2}. \quad (126)$$

For completeness, I quote the scaling violating terms (taken from [12]) up to terms of order $m_R^4 \ln m_R^2$

$$u_0 = 2 - \frac{m_R \sinh m_R}{2 \sinh^2 \frac{1}{2} m_R} - \frac{m_R \sinh m_R}{2 - \sinh^2 \frac{1}{2} m_R}, \quad (127)$$

$$u_1 = \beta_1 + m_R^2 \left\{ -2 \ln m_R^2 + N \left(\frac{7}{72} + \frac{\pi^2}{3} r_0 - \frac{4\pi^2}{9} r_1 - \frac{16\pi^2}{9} r_2 \right) \right. \\ \left. + \frac{13}{36} - \frac{\pi}{\sqrt{3}} + \frac{2\pi^2}{3} r_0 - \frac{112\pi^2}{9} r_1 + \frac{704\pi^2}{9} r_2 \right\} (16\pi^2)^{-1} \\ + \mathcal{O}(m_R^4 \ln m_R^2), \quad (128)$$

$$v_0 = -\frac{1}{4} \frac{m_R \sinh m_R}{2 - \sinh^2 \frac{1}{2} m_R}, \quad (129)$$

$$v_1 = m_R^2 \left\{ \frac{1}{48} (N+2) \ln m_R^2 + N \left(\frac{\pi^2}{3} r_0 + \frac{4\pi^2}{3} r_1 \right) + \frac{2\pi^2}{3} r_0 + \frac{8\pi^2}{9} r_1 \right. \\ \left. - \frac{64\pi^2}{9} r_2 + \frac{3\sqrt{3}\pi - 4}{12} \right\} (16\pi^2)^{-1} + \mathcal{O}(m_R^4 \ln m_R^2), \quad (130)$$

$$w_0 = \frac{m_R \sinh m_R \sinh^2 \frac{1}{2} m_R}{4 - \sinh^4 \frac{1}{2} m_R}, \quad (131)$$

$$w_1 = \delta_1 + m_R^2 \left\{ \frac{1}{12} (N+2) \ln m_R^2 + N \left(\frac{\pi^2}{3} r_0 + \frac{16\pi^2}{9} r_1 + \frac{16\pi^2}{9} r_2 - \frac{7}{72} \right) \right. \\ \left. + \frac{2\pi^2}{3} r_0 - \frac{32\pi^2}{9} r_1 - \frac{224\pi^2}{9} r_2 - \frac{5}{18} + \frac{\sqrt{3}\pi}{36} \right\} (16\pi^2)^{-1} \\ + \mathcal{O}(m_R^4 \ln m_R^2), \quad (132)$$

where the constants r_0, r_1, r_2 are given by

$$r_0 = 0.13823047, \quad (133)$$

$$r_1 = -0.04029906, \quad (134)$$

$$r_2 = 0.00763417. \quad (135)$$

For ϵ , the m_R -dependent expansion is written as

$$\epsilon(m_R, g_R) = \sum_{\nu=0}^{\infty} x_\nu(m_R) g_R^\nu, \quad (136)$$

with the coefficients

$$x_0 = \frac{\sinh m_R}{m_R} \frac{2 + \sinh^2 \frac{1}{2} m_R}{2 - \sinh^2 \frac{1}{2} m_R}, \quad (137)$$

$$x_1 = \epsilon_1 + m_R^2 \left\{ \ln m_R^2 + N \left(-\frac{1}{16} - \frac{\pi^2}{6} r_0 + \frac{2\pi^2}{9} r_1 + \frac{8\pi^2}{9} r_2 \right) \right. \\ \left. - \frac{\pi^2}{3} r_0 + \frac{20\pi^2}{3} r_1 - \frac{112\pi^2}{3} r_2 - \frac{11}{24} + \frac{7\sqrt{3}\pi}{36} \right\} (16\pi^2)^{-1} \\ + \mathcal{O}(m_R^4 \ln m_R^2). \quad (138)$$

References

- [1] H. Neuberger, Phys. Lett. B199 (1987) 536
- [2] M. Lüscher and P. Weisz, Nucl. Phys. B300[FS22] (1988) 325
- [3] M. Lüscher and P. Weisz, Nucl. Phys. B290[FS20] (1987) 25
- [4] M. Lüscher and P. Weisz, Nucl. Phys. B295[FS21] (1988) 65
- [5] M. Lüscher and P. Weisz, Nucl. Phys. B318 (1989) 705
- [6] R. Dashen and H. Neuberger, Phys. Rev. Lett. 50 (1983) 1897
- [7] K.G. Wilson, Phys. Rev. B4 (1971) 3184;
K.G. Wilson and J.B. Kogut, Phys. Rep. 12 (1974) 75;
M. Aizenman, Phys. Rev. Lett. 47 (1981) 1; Comm. Math. Phys. 86 (1982) 1;
J. Fröhlich, Nucl. Phys. B200 (1982) 281;
C.B. Lang, Phys. Lett. B155 (1985) 399; Nucl. Phys. B265[FS15] (1986) 630
- [8] For a review, see D.J.E. Callaway, Phys. Rep 167 (1988) 241
- [9] M. Lüscher and P. Weisz, Phys. Lett. B212 (1988) 472
- [10] J. Kuti, L. Lin and Y. Shen, Phys. Rev. Lett. 61 (1988) 678;
A. Hasenfratz, K. Jansen, J. Jersák, C.B. Lang, T. Neuhaus and H. Yoneyama, Nucl. Phys. B317 (1989) 81
- [11] For reviews, see for instance H. Neuberger, preprint RU-89-44;
H. Neuberger, *in* Lattice Higgs Workshop, ed. B. Berg et al. (World Scientific, Singapore, 1988)
- [12] G. Bhanot, K. Bitar, U.M. Heller and H. Neuberger, Nucl. Phys. B343 (1990) 467;
U.M. Heller, Nucl. Phys. B (Proc. Suppl.) 17 (1990) 649
- [13] G. Bhanot, K. Bitar, U.M. Heller and H. Neuberger, Nucl. Phys. B353 (1991) 551;
erratum Nucl. Phys. B375 (1992) 503;
U.M. Heller, H. Neuberger and P. Vranas, Phys. Lett. B283 (1992) 335
- [14] U.M. Heller, M. Klomfass, H. Neuberger and P. Vranas, preprint FSU-SCRI-93-29,
Nucl. Phys. B, in press
- [15] M. Klomfass, Ph.D. Dissertation, preprint FSU-SCRI-92T-117
- [16] M. Klomfass, Nucl. Phys. B (Proc. Suppl.) 30 (1993) 690
- [17] M. Wortis, Linked Cluster Expansion, *in* Phase Transitions and Critical Phenomena,
Vol. 3, ed. C. Domb and M.S. Green (Academic Press, London, 1974)
- [18] D.S. Gaunt, M.F. Sykes and S. McKenzie, J. Phys. A12 (1979) 871

- [19] G.A. Baker and J.M. Kincaid, J. Stat. Phys. 24 (1981) 469
- [20] M.A. Moore, Phys. Rev. B1 (1970) 2238